

Channel Dynamics in an Experimental Alluvial Fan Under Constant Boundary Conditions: A Classification of Avulsion and Lateral Migration Events

Abstract

Alluvial fans exhibit complex channel dynamics, spanning gradual lateral migration to sudden avulsions. Although allogenic processes are recognized as key drivers of these behaviors, the autogenic mechanisms regulating channel change remain poorly understood. In this study, we present a quantitative analysis of the main channel kinematics on a widely graded, non-cohesive experimental alluvial fan, utilizing high-temporal-resolution RGB imagery and main channel centerline tracking. By employing two key metrics—displacement magnitude (normalized by channel width) and flow continuity, defined as the degree of overlap in the active channel footprint from one image to the next—we move beyond qualitative assessments, which are often subject to researcher bias, and establish a clear framework for distinguishing between migratory (continuous) and avulsive (discrete) channel behaviors. Our findings reveal that the fan alternates between intervals of concentrated channel activity, when a small number of channels route sediment efficiently toward the fan toe, and intervals of distributed channel activity, when a more complex channel network promotes mid-fan sediment storage and abrupt reorganization (i.e., avulsions). Contrary to the conventional assumption that systematic aggradation from toe to apex triggers large-scale channel abandonment, our results show that lateral sediment redistribution can interact with vertical aggradation by repeatedly reworking sediment within the active corridor, potentially prolonging the interval before major channel abandonment occurs. These results highlight the critical role of self-regulating autogenic processes, particularly the lateral reworking of coarse sediment, in controlling both the timing and scale of channel adjustments, and emphasize the importance of incorporating localized feedbacks into models of alluvial-fan dynamics.

Depositional environments such as alluvial fans and fan deltas often exhibit a quasi-radial pattern of deposition created by the spreading of incoming sediment in response to reduced confinement, slope transitions, and changing boundary conditions (Harvey 2010; Bull 1979; Mackey and Bridge 1995). Superimposed on this fan-scale geometry, a dynamic network of active channels migrates laterally and occasionally undergoes abrupt relocation, shaping overall fan morphology (Jerolmack and Mohrig 2007; Jobe, Howes, and Auchter 2016; Slingerland and Smith 2004).

Across many depositional systems, short-lived channel adjustments—such as bar migration, bank erosion, or shifts in individual flow threads—are confined to a narrow corridor of activity only a few channel widths wide, commonly referred to as the channel belt. These localized adjustments operate continuously and incrementally, redistributing sediment without necessarily reorganizing the fan surface (P. Ashmore 2013). Over longer timescales, however, the repeated lateral motion can accumulate so that reworking spreads beyond the channel belt, and affects a large portion of the fan surface (Cazanacli, Paola, and Singh 2022). By contrast, avulsions represent discrete, abrupt changes in which

a channel abandons its established corridor and relocates to a new course (Mohrig et al. 2000; P. E. Ashmore 1991). Avulsions may be spatially limited, as in localized avulsions where flow is diverted into an adjacent chute or braid thread, or fan-scale, as in major avulsions that initiate the growth of a new lobe. Bifurcation, the division of flow into two or more downstream branches, often acts as a decision point between different modes of channel adjustment. When bifurcations are stable, multiple threads can coexist and migrate incrementally, whereas unstable bifurcations typically result in one branch capturing flow, leading to channel abandonment and avulsion (Burge 2006).

Conventional studies suggest that avulsion is typically driven by two key processes: (1) superelevation, where in-channel sediment aggradation exceeds that of the surrounding floodplain, progressively raising the channel relative to adjacent floodplain, and (2) backfilling, in which upstream-migrating waves of sediment reduce channel capacity, promoting overflow into a new pathway (Mohrig et al. 2000; Bryant, Falk, and Paola 1995; Clarke, Quine, and Nicholas 2010; Reitz, Jerolmack, and Swenson 2010). Both mechanisms imply that avulsion frequency is often tied to the time required to fill a channel with sediment. For a given channel depth, the avulsion timescale is proportional to the channel depth and inversely related to the aggradation rate (Jerolmack and Mohrig 2007). Recent work also demonstrates that channel relocation need not be abrupt. Instead, channels can shift progressively through a sequence of lateral adjustments, a process termed sweeping (Sylvester, Durkin, and Covault 2019; Cazanacchi, Paola, and Singh 2022). Under this interpretation, repeated small lateral shifts can integrate over time into a net relocation, so channel abandonment can emerge from sustained migration rather than a single threshold-style jump

From a stratigraphic perspective, changes in channel position—whether gradual or abrupt—are critical for redistributing water and sediment across floodplains, ultimately shaping fluvial architectures. However, from a geohazard standpoint, distinguishing between these processes is essential because each responds differently to environmental factors such as sea-level rise and variations in sediment supply (Jerolmack and Mohrig 2007; Slingerland and Smith 2004; Harvey 2010). For instance, sea-level rise can promote delta-top aggradation and increase channel avulsion rates, as demonstrated by laboratory experiments (Jerolmack 2009; Martin et al. 2009). In contrast, studies of non-avulsive settings show that channel migration rates may remain stable or even decline during sea-level rise (Bufer et al. 2019; Wickert et al. 2013). Instead, these areas often exhibit migration patterns that are more sensitive to changes in downstream sediment flux (Constantine et al. 2014; Wickert et al. 2013).

Both internal (autogenic) and external (allogenic) factors shape channel evolution on alluvial fans (Schumm, Mosley, and Weaver 1987; Clarke, Quine, and Nicholas 2010; Reitz and Jerolmack 2012). Autogenic processes include local changes in slope, sediment deposition, and channel geometry that self-organize within the fan, whereas allogenic forces—such as climatic shifts, tectonics, and human interventions—induce broader environmental changes that alter flow conditions. Much of our understanding about fan dynamics, particularly autogenic behavior, comes from experiments and field studies, but

many interpretations have historically been qualitative. Early laboratory and field studies (e.g., (Schumm, Mosley, and Weaver 1987; Whipple et al. 1998; Hooke 1968)) relied on visual observations and sparse measurement grids, providing pioneering but coarse-resolution insights into fan-building processes. In recent years, high-resolution topographic surveys (Miller, Kim, and McElroy 2019; Reitz and Jerolmack 2012) have provided finer spatial detail; however, their relatively coarse temporal sampling (on the order of 15 minutes) still misses many short-lived changes. More recently, using high-frequency, high-resolution topographic data, Leenman and Eaton (2021) captured the complex nature of fan behavior beyond period cycles; however, distinguishing gradual channel migration from abrupt channel relocation remains challenging due to their pixel-based wet/dry event classification.

Several image-based motion-tracking approaches have been developed to quantify channel displacement in fluvial systems. Chadwick et al. (2022) applied Particle Image Velocimetry (PIV) to a laboratory delta experiment and subsequently extended the framework to natural rivers using Landsat imagery (Chadwick et al., 2023). PIV estimates displacement by cross-correlating image patches between successive time steps, which requires the same features to remain recognizable within the search window. This makes the method effective for gradual channel migration, but abrupt relocations such as avulsions may move or remove the original texture, making them difficult to detect reliably. Sylvester et al. (2019) used Dynamic Time Warping (DTW) to quantify lateral migration rates along meandering river centerlines, and Li and Limaye (2025) extended this approach to individual threads of the braided Brahmaputra-Jamuna River using annual Landsat composites. Although DTW is useful for comparing continuously traceable centerlines, it is less appropriate where the main channel changes length or reorganizes in several locations between observations. In these cases, the optimal DTW alignment may pair points that are close in plan view but do not represent the same radial position or the same part of the channel system, which is problematic in a fan setting. Image-stacking methods have also been used to map channel mobility from long-term water-occurrence records and distinguish persistent from transient channel corridors (Lee et al., 2022). These methods capture the accumulated pattern of channel mobility over longer periods, but in an analogous experimental setting where channels change rapidly and multiple adjustments occur in short succession, stacking would merge short-lived events and make it difficult to recover the timing and sequence of individual migration and avulsion episodes.

Commented [n1]: This paragraph was added in response to Reviewer 2's first comment.

Another limitation in many fan experiments is the simplification of the sediment. Many experimental studies of alluvial fans have used narrowly graded sediment mixtures (sand-only or bimodal setups), thereby reducing the wide grain-size variability observed in natural fans (e.g., (Schumm, Mosley, and Weaver 1987; Reitz and Jerolmack 2012; Reitz, Jerolmack, and Swenson 2010). Such mixtures can reproduce fan building at a basic level; however, they often underrepresent mechanical interlocking that occurs with a broad range of grain sizes, resulting in channels with easily erodible margins that tend to form

unconfined sheet flow. Consistent with this, Booker and Eaton (2020) demonstrated that narrowly graded mixtures cannot reproduce the morphodynamics observed in a widely graded mixture with the same median grain size D_{50} .

This study investigates the dynamics of a widely graded experimental alluvial fan constructed under constant discharge and sediment supply, focusing on the displacement of the main channel over time and space. While smaller side channels might fill more quickly and be more prone to shift, the changes they induce are relatively localized and less significant in reshaping the fan's large-scale structure compared to the main channel. This is analogous to the concept of "formative flow" described by Davidson and Eaton (2018), in which larger, less frequent flows shape channel form, whereas "effective flows" transport most sediment over time but have a lesser impact on morphology (Wolman 1960). By tracking channel displacement at high temporal resolution (every minute), we establish a conceptual framework for distinguishing gradual, bank-erosion-driven channel migrations (continuous in both time and space) from abrupt, avulsive relocations (discrete shifts in channel position). Our primary question is how often the channel migrates gradually versus avulsing abruptly under these steady-input but highly dynamic conditions. We hypothesize that continuous sediment redistribution within a confined corridor inhibits the bed aggradation needed for sudden, discrete channel reoccupation elsewhere on the fan.

To test this, we map the main flow path in each image at one-minute intervals and quantify both the magnitude and direction of channel displacement. We then compare the cumulative net shifts associated with gradual migration to the single, larger displacements that define avulsions, thereby clarifying whether the channel shifts abruptly due to localized deposition or more diffuse erosion. This approach provides a more explicit link between how the main channel reworks the fan surface and why such reworking occurs under steady conditions, offering new insights into the autogenic processes that control fan evolution. By clarifying the interplay between gradual and abrupt channel shifts, these findings facilitate more accurate stratigraphic interpretations of fan deposits and enhance hazard assessments in settings prone to rapid channel reconfiguration.

1 Methods

1.1 Experimental Set-up

We conducted the experiment using a physical model representing a typical gravel-cobble alluvial fan at the University of British Columbia. We used a fan table with dimensions of 2.4 meters by 2.4 meters and a height of 0.2 meters. The table was equipped with a feeder channel, which measured 0.2 meters by 0.5 meters by 0.18 meters, centrally located along one wall of the table and a conveyor belt sediment feeder next to it (as shown in Fig.). Water was supplied from a constant-head tank with adjustable outflow. Sediment and

water were mixed in a funnel and delivered to the feeder-channel inlet. We allowed sediment to aggrade and degrade freely in the feeder channel, as in a natural system. The discharge and sediment supply were held constant at 100 mL/s and 2 g/s, respectively, throughout the experiment, resulting in a sediment concentration of 1.1% by volume, characteristic of clear-water floods rather than debris-flow conditions (Church and Jakob 2020). We set the fan table gradient at 0.01 (m/m) to ensure efficient drainage away from the fan's edge. The sediment mixture was widely graded (0.25–8 mm), with a median size D_{50} of 0.6 mm and D_{95} of 2.3 mm (Fig.). The experiment ran for a total of 9 hours. The first 3.5 hours served as a baseline setup period, after which we began detailed observation and analysis of fan development and channel dynamics.

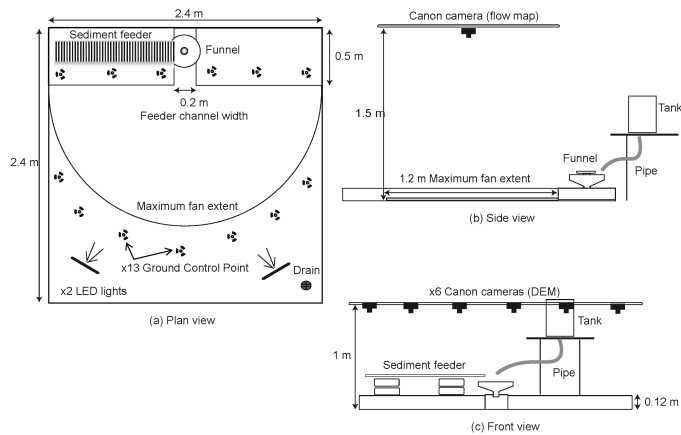


Figure 1.1: Experimental setup: (a) plan view, (b) side view, and (c) front view.

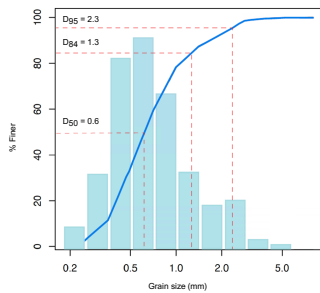


Figure 1.2: Grain size distribution (GSD) of the sand and fine gravel mixture in the experiments.

1.2 Analysis

We briefly summarize our data-processing workflow here. Optical flow analyses were performed in Python using OpenCV (Bradski 2000), while all other analyses were conducted in R (R Core Team 2025). All scripts, along with a representative subset of the experimental dataset, are available in our GitHub repository:

<https://github.com/Nastaranmt?tab=repositories>.

1.2.1 Data Collection and Optical Flow Analysis

We used a centrally mounted overhead camera system positioned above the fan table to capture images every three seconds throughout the experiment, achieving a spatial resolution of 1 mm per pixel, to document the structure of the flow with high temporal resolution, capturing images every three seconds throughout the experiment. These images were compiled into one-minute time-lapse videos, each containing 20 frames. The resulting active flow footprint therefore represents the cumulative area occupied by flow during the full one-minute interval. To identify active flow zones, we applied Farnebäck dense optical flow (FDOF) (Farneback 2000), which estimates pixel-wise motion between consecutive frames based on two assumptions: (1) gray-level constancy, where pixel intensities remain stable over short intervals, and (2) velocity smoothness, where neighboring pixels exhibit similar motion. FDOF minimizes the intensity difference between successive frames, as expressed by the following equation:

\$\$

where $I_1(x)$ and $I_2(x)$ are the intensity values at position x in the first and second frames, respectively, and d is the displacement vector (Farneback 2000). We implemented the algorithm in Python using OpenCV's `cv2.calcOpticalFlowFarneback` function. Before calculating flow, each frame was converted to grayscale and smoothed with a 5×5 Gaussian kernel to reduce noise. The parameters used are summarized in Table 1.

The algorithm produces a dense field of motion vectors, where each pixel is assigned a vector $v = (u, v)$, representing its estimated displacement between two consecutive frames. From this vector, both the magnitude and direction of motion are derived as:

$$\begin{aligned} |v| &= \sqrt{u^2 + v^2}, \\ \theta &= \arctan\left(\frac{v}{u}\right). \end{aligned}$$

For each one-minute sequence (20 frames), we computed 19 frame-to-frame flow fields and averaged per-pixel magnitudes to obtain a mean-motion raster, $\overline{|u|}$. Dense optical flow is highly sensitive to sub-pixel intensity changes, which means it can also detect low-amplitude noise in areas where flow is slow or ponded, but it produces stronger motion signals and thus higher contrast in regions of actively flowing water. Initial tests showed that applying a 75th-percentile threshold to $\overline{|u|}$ preserved active cells while filtering out quasi-static water patches that color-thresholding misclassifies as active (Leenman and

Eaton 2021). Based on these tests, we implemented a two-step thresholding in which we first retained only those pixels where $\overline{|\mathbf{u}|} \geq Q_{0.75}$, and then performed clump-based segmentation to remove small, isolated pixel clusters (Fig. 3).

Although our primary analyses relied on overhead imagery and optical flow techniques, we also generated digital elevation models (DEMs) to validate and contextualize our observations. DEMs were created using an adaptation of Structure-from-Motion (SfM) photogrammetry (Fonstad et al. 2013; Westoby et al. 2012). Six Canon EOS Rebel T6i DSLRs with EF-S 18–55 mm lenses were mounted on a rail system above the table, taking photos every 10 cm with at least 85% stereo overlap. Photographs were acquired at 30-minute intervals after stopping the water flow and allowing the fan surface to drain. Thirteen ground control points ensured accurate georeferencing of the DEMs, achieving a resolution of 0.5 mm (details about the photogrammetry methods are provided in the supplementary material).

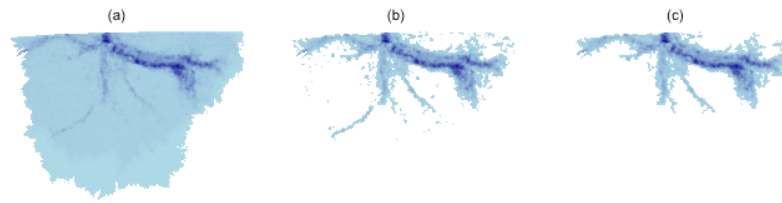
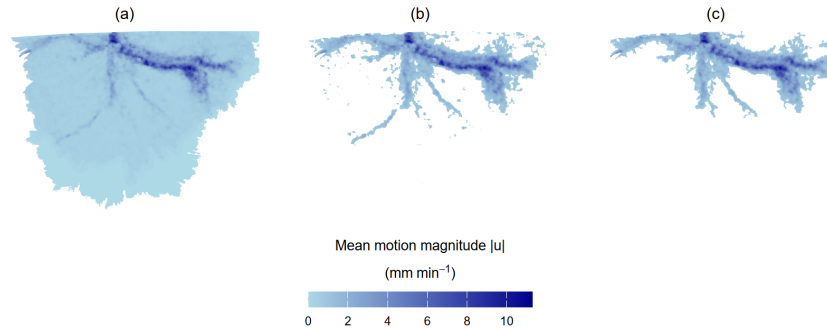


Figure 1.3: Visualization of active flow areas on the alluvial fan using Farneback optical flow analysis. (a) Raw optical flow motion values representing the magnitude of per-pixel displacement (in mm per frame) averaged over one-minute intervals; warmer blue tones indicate higher motion magnitudes. (b) Thresholding at the 0.75 quantile to isolate significant flow activity. (c) Final flow map after removing noise through clump-based segmentation. Color scale in all panels represents motion magnitude; direction of motion is not shown here but is used separately in the displacement analysis (Section 2.2.3).



1.2.2 Channel network detection

To define the centerlines of geomorphically active channels on the fan, we generated semicircular contour lines spaced at 2 cm intervals from the fan apex to the toe (Fig. 4 (a)) and extracted flow raster values along each contour line (Fig. 4 (b)). We then applied the Density-Based Spatial Clustering of Applications with Noise (DBSCAN) algorithm in two stages. In the first stage, DBSCAN was applied along each semicircular contour to group points within a 2 cm neighborhood into clusters, representing individual channel transects (Fig. 4 (c)). For each transect, we considered the motion magnitude of pixels within the channel and calculated the centroid of each cluster to approximate the thalweg location (fig. 4 (c)). In the second stage, DBSCAN was applied to these centroids along the radial direction of the fan. By clustering centroids within a 2 cm radius, we connected individual channel transects into continuous paths, representing channel segments (Fig. 4 (d, e)).

Further, the channel segments were connected based on their proximity, with the starting point of each channel segment linked to its nearest upstream neighboring channel segment. Channels were then labelled according to their Total Motion Contribution (TMC), calculated as the product of the average pixel motion and the total length of a channel, a proxy for the size of the channel (i.e. the volume of sediment transported and/or the volume of water carried in it). The channel with the highest TMC was designated as the main channel, with channel order increasing as average motion decreased, as shown in Figure 4 (f).

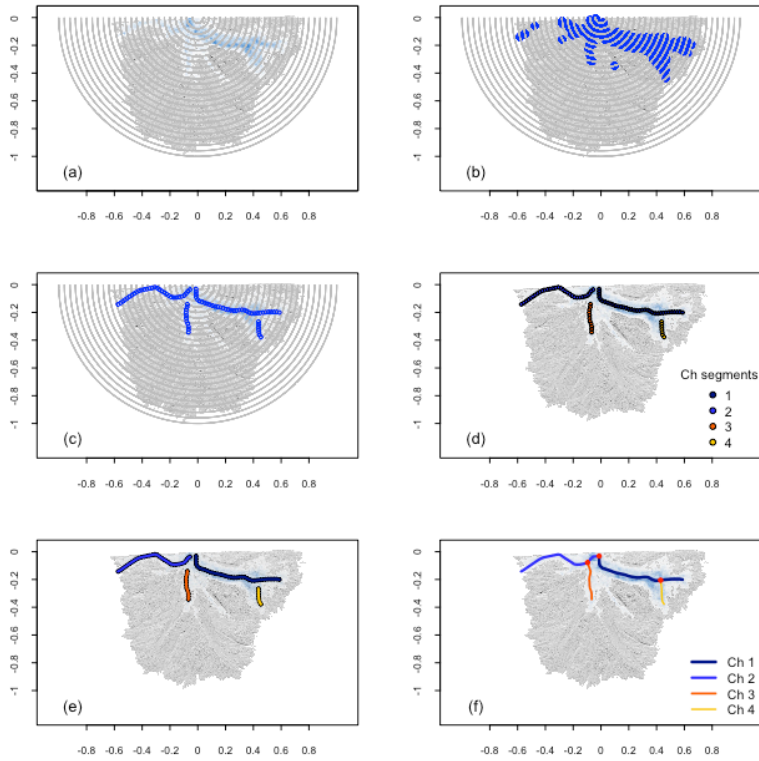


Figure 1.4: Channel detection and clustering on an experimental alluvial fan. (a) Initial flow data with semicircular contour lines (gray). (b) Result of adaptive thresholding, showing high-motion pixels above the average in each radial section. (c) Channel transects identified using DBSCAN clustering, with centroids marking the midpoints of each transect. (d) Final clustering of centroids to form continuous channel paths, with color-coded clusters representing distinct channels from the apex to the distal edge. Channel network detection steps: (a) semicircular contour lines at 2 cm intervals (gray); (b) high-motion pixels in each radial section; (c) channel transects identified using DBSCAN clustering, with centroids marking the midpoints of each transect; (d) clustering of centroids to form continuous channel segments (shown as points); (e) connected channel segments within each cluster shown as lines; (f) channel segments connected to their nearest upstream neighbour and ranked by Total Motion Contribution (TMC), with channel order increasing as average motion decreases.

1.2.3 Main Channel Displacement Magnitude and Direction

To analyze the main channel displacement over time, the angular position of a point at two time steps (t_1 and t_2) is calculated as $\theta_1 = \arctan2(Y_{t1}, X_{t1})$ and $\theta_2 = \arctan2(Y_{t2}, X_{t2})$. The angular displacement, $\Delta\theta$, is then computed as the absolute difference between these angular positions: $\Delta\theta = |\theta_2 - \theta_1|$. Since angular measurements are bounded within the range $-\pi$ to π , any displacement exceeding π is adjusted to fall within $[0, \pi]$ using the rule: $\Delta\theta = 2\pi - \Delta\theta$ if $\Delta\theta > \pi$, otherwise $\Delta\theta$ remains unchanged.

The direction of movement is determined using the signed value of $\Delta\theta$, where positive values indicate counterclockwise movement, and negative values indicate clockwise movement. The magnitude of displacement, expressed in units of channel length, is then calculated as the arc length $\text{Arc_Length} = r \cdot \Delta\theta$, where r represents the radial distance of the point from the apex (Fig. 5 (a)). The buffer width was determined by dividing the average flow width/the number of full length channels. The width of the main channel was calculated by dividing the area of active flow cells within the buffer by the length of the main channel (Fig. 5 (b)).

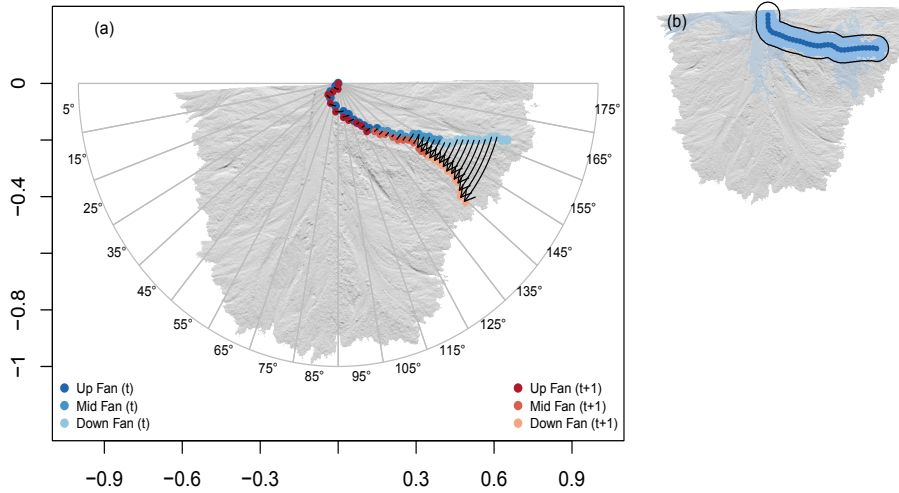


Figure 1.5: (a) Angular displacement of the main channel between minutes 216 and 217, overlaid on a hillshaded DEM acquired at the subsequent 30-minute scan. (b) Channel width estimates derived from buffered flow zones for the same time interval, overlaid on the same hillshaded DEM.

2 Result

2.1 Qualitative Observation

Throughout the 5.5 hours of the experiment, the flow zone appeared to migrate continuously, with variability in both timing and spatial extent. Based on visual inspection of time-lapse videos (see Supplementary Video) corresponding to the 5.5-hour experiment, we noted three qualitative patterns: (1) The main channel moved back and forth across different parts of the fan, occasionally sweeping over long distances before reversing direction. During these shifts, the channel oscillated in small steps while showing a net drift in one direction, either clockwise or counterclockwise. (2) Certain portions of the channel, particularly in the lower fan region, exhibited more pronounced lateral movement than others. (3) The upper segment near the apex, by contrast, remained comparatively stable, although minor realignments still occurred intermittently.

2.2 Main channel displacement

To characterize the spatial and temporal behavior of the main channel, we quantified the active flow route's displacement in time and space. Specifically, we define $\Delta\theta$ as the instantaneous angular change of the channel centerline between consecutive images (recorded at one-minute intervals), with units of degrees per minute. $\Delta\theta$ is a proxy for the migration rate that accounts for fan geometry by expressing displacement as an angular change about the apex. Where necessary, we convert the angular shift into an equivalent displacement expressed in mean channel widths.

Figure (a) displays $\Delta\theta$ for the up fan, mid fan, and down-fan sectors. The difference in angular shift distribution among the three locations indicates that the channel has a fairly complex mobility, with different sections moving at different rates. Furthermore, different parts of the channel (e.g., up-fan vs. down-fan) do not always move in the same direction. Additionally, the magnitude and variability of these shifts increase with distance from the apex. Near the apex, $\Delta\theta$ has smaller mean values (approximately 2° min^{-1}) with a standard deviation of $\pm 4^\circ$, indicating frequent but minor channel displacements. In contrast, the mid-fan and down-fan regions exhibit larger and more variable shifts (standard deviations up to $\pm 7^\circ$), signifying greater channel instability and larger reworking events farther from the apex.

Within this mobile fan system, the $\Delta\theta$ time series alternates between two distinct patterns: low-mobility intervals (stable to slight displacement) and high-mobility intervals. The Low Mobility intervals, highlighted in gray in Figure (a), occur when the main channel's average angular displacement falls below approximately $1.32^\circ \text{ min}^{-1}$. These intervals often last for several minutes (sometimes up to 24 minutes, on average around 5 minutes), during which the channel occupies a relatively narrow corridor with negligible lateral movement. This behavior typically indicates near-equilibrium conditions, where the channel is effectively incised, transporting sediment efficiently, and any coarse or bar deposits remain small enough to be reworked quickly. Outside these low mobility intervals, the channel moves

more rapidly at rates above $1.32^\circ, \text{min}^{-1}$, often reversing direction and/or shifting over larger distances.

Figure (b) shows the cumulative signed angular displacement $\Sigma\Delta\theta$, where positive slopes indicate counterclockwise shifts, and negative slopes represent clockwise movement. Near-horizontal segments correspond to low-mobility intervals during which the channel's net position remains largely confined and stable. By contrast, more moderate slopes suggest steady directional migration, and steep slopes reflect rapid realignments, which may reflect either continuous lateral migration, where the channel sweeps several sectors during the one-minute interval, reworking all sediment along its path, or abrupt avulsion, where the channel jumps to a new route, bypassing the previous corridor. Distinguishing between these mechanisms (continuous vs. discrete) requires additional analysis beyond the cumulative signal alone.

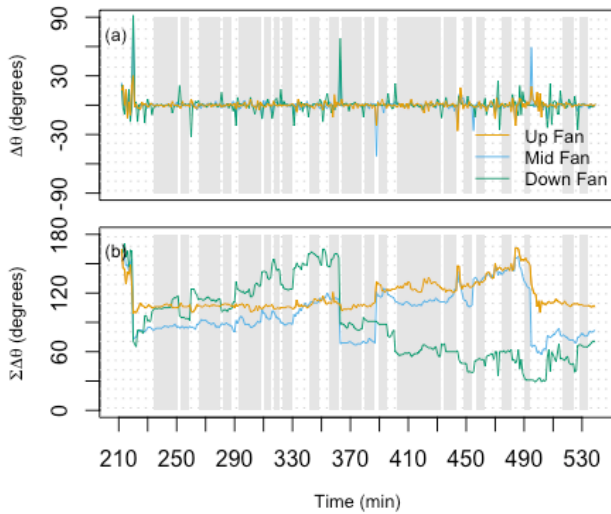


Figure 6: Time-resolved angular displacement of the main channel: (a) instantaneous angular displacement for the up-fan, mid-fan, and down-fan sectors, with gray-shaded periods denoting low-mobility intervals, (b) cumulative signed angular displacement, where positive slopes indicate counterclockwise shifts and negative slopes represent clockwise shifts.

2.3 Avulsion Classification Scheme

Building on the spatial and temporal patterns quantified above, we introduce a classification framework that separates the observed channel shifts into distinct behavioral types. We evaluate each channel shift according to:

- (1) the arc length of channel displacement, normalized by a time-varying, experiment-wide average channel width (updated each minute),
- (2) the length of the channel affected, and
- (3) the mechanism of change (continuous vs. discrete).

We classified channel displacement using three thresholds. Shifts less than or equal to 0.25 of the average channel width were considered negligible, displacements between 0.25 and 1.0 indicated moderate change, and those exceeding 1.0 times the channel width indicated a high degree of channel relocation. The mechanism of change was determined by the degree of overlap in flow cells between consecutive images. Fewer than 80% overlap implies a discrete (avulsive) jump, whereas higher overlap indicates continuous lateral migration (Fig.).

Based on the section-wise classification, fan-scale behavior was determined by combining changes across the up-fan, mid-fan, and down-fan sections. Table 1 summarizes three avulsion modes— complete, partial, and localized— based on whether high-magnitude, discrete displacements (>1.0 channel widths) affect one, two, or all three fan sections. A similar threefold classification applies to lateral migrations when displacements exceed 0.25 channel widths but maintain continuity above 80% from one time step to the next.

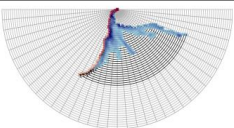
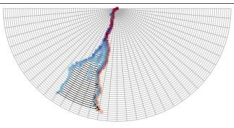
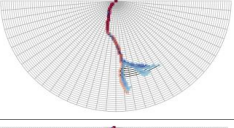
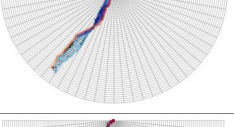
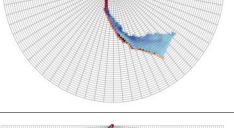
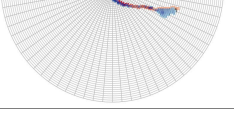
Behavior	Length affected	Displacement (times channel width)	Change type	Example
Complete Avulsion	$\geq 2/3$	> 1.0	Discrete	
Partial Avulsion	$< 2/3$ $\geq 1/3$	> 1.0	Discrete	
Localized Avulsion	$< 1/3$	> 1.0	Discrete	
Complete Lateral Migration	$\geq 2/3$	≥ 0.25	Continuous	
Partial Lateral Migration	$< 2/3$ $\geq 1/3$	≥ 0.25	Continuous	
Localized Lateral	$< 1/3$	≥ 0.25	Continuous	

Figure 7: Classification framework for avulsion and lateral migration events on the experimental alluvial fan. Events are distinguished using displacement magnitude normalized by channel width, flow-path continuity between successive active-flow footprints, and the length of the main channel affected. Low-overlap, discrete shifts are classified as avulsions, whereas high-overlap, continuous shifts are classified as lateral migrations. Complete, partial, and localized modes indicate the spatial extent of the affected channel length. Classification of avulsion and lateral migration modes on experimental alluvial fan.

2.4 Channel Displacement Statistics and Physical Interpretation

Table 2 summarizes the frequency and displacement statistics for each classified channel behavior, listed in order of ~~decreasing~~increasing mean displacement. Complete avulsions (four events) show the largest average shift (~ 3 channel widths) and highest variability

(± 2.90), while partial avulsions (15 events) are more frequent, with moderate mean shifts (~ 1.04). In contrast, localized avulsions and complete lateral migrations both remain below 1.0 channel width (0.55 and 0.74, respectively), consistent with cases where either (1) a single sector experiences a short but intense jump, or (2) the fan undergoes more continuous reworking without fully abandoning its corridor. Partial and localized lateral migrations exhibit even smaller displacements (0.43 and 0.21), whereas quasi-stable conditions account for just over half (53%) of all observations, with a mean displacement of 0.08.

To examine the buildup of smaller, cumulative shifts between avulsions, we tracked cumulative normalized displacement in each fan sector (Fig.). After every complete or partial avulsion (i.e., a major reorganization affecting at least two fan sectors), this cumulative sum was reset to zero to delineate the onset of a new “fan reorganization” phase. Localized avulsions were excluded from the reset criterion because they affect only one sector and thus do not fully re-route the main channel. Between 260 min and 350 min, the main channel’s cumulative displacement in the mid-fan/down-fan sectors reached up to ~ 4.93 channel widths—comparable to a major avulsion in total net shift. Although no single one-minute lateral migration event exceeded the displacement typically associated with an avulsion, over longer timescales, cumulative lateral migration can produce spatial changes on par with those triggered by avulsions.

A comparison of net area changes over two 30-minute intervals—a lateral-migration phase (260–300 min) and an avulsion-dominated phase (450–480 min)—reveals that the absolute area of geomorphic change is 0.33 m^2 vs. 0.41 m^2 , respectively (Fig.). When these values are normalized by the total fan area (1.18 m^2 vs. 1.57 m^2), the corresponding proportions are approximately 28% vs. 26%. Despite the frequent assumption that avulsions produce a more extensive geomorphic footprint, these data indicate that lateral migration can rework a comparably large fraction of the fan surface within the same time frame.

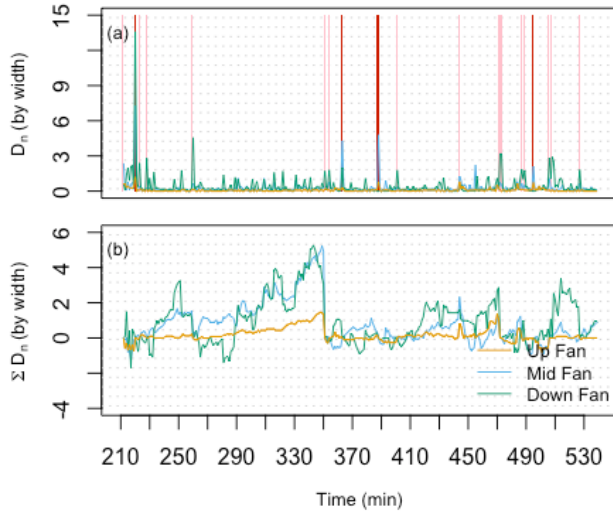


Figure 8: Normalized displacement (D_n) and cumulative Shifts: (a) time series of the per-minute normalized displacement (in each fan sector. Vertical red and pink lines mark complete and partial avulsions, respectively. (b) Cumulative normalized displacement in each sector, reset to zero after complete or partial avulsions that affect at least two sectors.

2.5 Avulsion Timing and State Dependence

Major avulsions (complete or partial; $n = 19$) were identified from the event classification, and their occurrence times were used to compute inter-event intervals Δt . Intervals were highly variable (range = 1–91 minutes; median = 10 minutes; mean = 17.5 minutes), indicating that major avulsions do not exhibit a single characteristic recurrence time over the analyzed interval.

Rather than treating the event series as stationary, we evaluated avulsion timing in relation to the mobility state of the main channel. Using the mobility threshold defined in Section 2.2, the record contains $T_{\text{high}} = 63$ high-mobility minutes and $T_{\text{low}} = 265$ low-mobility minutes (i.e., high mobility occupies $\sim 19\%$ of the time series). All major avulsions occurred during high-mobility minutes ($N_{\text{high}} = 19$, showing that major reorganizations are concentrated into brief high-mobility windows. Importantly, high mobility is not synonymous with major avulsion: only $\sim 30\%$ of high-mobility minutes correspond to major avulsion events ($19/63$). This framing clarifies the appearance of short clusters in the event sequence: closely spaced avulsions occur when high-mobility conditions persist across multiple consecutive minutes, whereas extended low-mobility intervals separate these windows. Because the mobility state is defined from the displacement metric $\Delta\theta$,

this conditioning is not intended as an independent mechanistic test; instead, it provides a compact way to show that major avulsions are confined to a small fraction of the run and occur within short episodes of elevated channel motion.

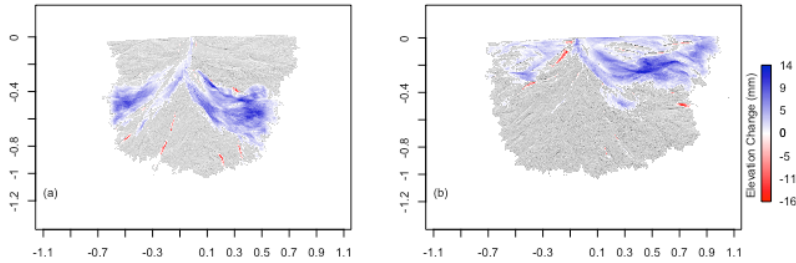


Figure 9: Geomorphic changes for (a) lateral migration from min 270 to 300 min, and (b) avulsion-dominated phases from 450 and 480 min, both overlaid on a hillshade DEM acquired at the subsequent 30-minute scan.

3 Discussion

3.1 Overview of Experimental Fan Evolution and Key Observations

Our principal aims in this study were to: (1) characterize the evolution of a widely graded, non-cohesive alluvial fan under constant boundary conditions, with a focus on the interplay of supply-limited and transport-limited regimes, (2) distinguish discrete (avulsive) relocations from continuous (migratory) shifts using a classification framework that combines displacement magnitude, flow-path continuity, and the spatial extent of reorganization, and (3) assess the timescales of fan-scale reorganizations, exploring whether large-scale avulsions follow predictable cycles or arise spontaneously from autogenic processes. In the following sections, we integrate these findings with existing models of fan-building processes, discussing the role of self-regulating autogenic feedback in driving alluvial-fan evolution.

Our non-cohesive, widely graded experimental alluvial fan reproduced several behaviors reported in earlier fan studies (Schumm et al., 1987; Zarn & Davies, 1994; Bryant et al., 1995; Whipple et al., 1998; Cazanaceli et al., 2002), including radial sediment dispersal, episodic channel reorganization, and internally generated (autogenic) variability. At the same time, the broader grain-size range and minute-scale tracking used here resolve short-lived shifts that are difficult to capture in more coarsely sampled experiments.

In our experiment, major avulsions did not exhibit a single recurrence timescale: inter-event intervals were highly variable (1–91 min; median 10 min; mean 17.5 min). When event timing is viewed alongside channel mobility, major avulsions are concentrated within brief high-mobility episodes. High mobility accounts for ~19% of the record (63 of 328

minutes) and contains all 19 major avulsions, while extended low-mobility intervals separate these episodes. Importantly, high mobility is not equivalent to major avulsion—only ~30% of high-mobility minutes coincide with major avulsion events—so elevated mobility appears to be a prerequisite for major reorganization but does not by itself determine whether a major avulsion occurs. The absence of a characteristic recurrence time and the concentration of events into short mobility episodes argue against a simple, regular cycle controlled solely by fan geometry. This interpretation is consistent with results from Leenman & Eaton (2021) and with broader evidence that constant boundary conditions can still produce nonlinear fan evolution (Muto & Steel, 2001).

3.2 A Unified Framework for Classifying Channel Behavior

Despite extensive experimental work on alluvial fans, quantitative frameworks for distinguishing different types of channel shifts remain limited. Earlier studies, such as Schumm et al. (1987), described large reorganizations but offered limited metrics for smaller, localized events. Later studies (Jerolmack, 2009; Reitz & Jerolmack, 2012) recognized the importance of both abrupt (avulsive) and gradual (migratory) processes but lacked a standardized approach for comparing results across experiments. In this study, we provide a quantitative classification framework for rapidly evolving channel networks observed at sufficiently high temporal resolution to capture intermediate channel positions, such as those collected in experimental settings or through repeat UAV surveys. The framework distinguishes between avulsive (discrete) and lateral (continuous) channel changes using two main parameters: displacement magnitude, measured in multiples of channel width and continuity, defined as the degree of overlap with the previous channel path. Based on quantitative thresholds for channel displacement and flow continuity, translating subjective observations into reproducible categories making it easier to achieve consistent experimental analyses and investigate the underlying physical processes.

Commented [n2]: Modified in response to the reviewer's second major comment.

A common view in fluvial systems is that sediment aggradation within, or around, the active channel “perches” the flow above the surrounding floodplain, preconditioning it for avulsion (Mohrig et al. 2000). Our experiment does not directly test this vertical mechanism because we did not track channel-bed elevation relative to the surrounding fan surface. What our classification scheme does show is that, in the highly dynamic system modelled here, large cumulative spatial displacements can arise from repeated lateral migration rather than from a single abrupt channel relocation. Thus, in this experiment, deposition and channel mobility interacted in a way that did not always lead to full channel abandonment. Between 260 and 350 minutes, for example, the main channel in our experiment underwent multiple corridor-scale sweeps in the mid-fan/down-fan region, cumulatively reaching ~4.93 channel widths—on par with a major avulsion in total displacement. Yet However, these repeated lateral shifts did not involve a sudden reoccupation of a completely different route. Instead, partial migrations and localized reworking repeatedly redistributed sediment within the active corridor, suggesting that

lateral mobility may have limited the development of a persistent perched channel in this experiment. . This interpretation is consistent with @cazanacli_sediment_2022, who suggest that highly dynamic, high-sediment-flux systems can sustain lateral migration as aggradation proceeds, redistributing sediment before sufficient vertical relief develops to trigger avulsion. Vertical preconditioning by aggradation and cumulative lateral displacement through migration are therefore not mutually exclusive. Their relative importance likely depends on the sediment-flux and lateral-mobility regime of the system, with highly dynamic, bedload-dominated fans potentially remaining in a sweeping-dominated state even as aggradation continues.

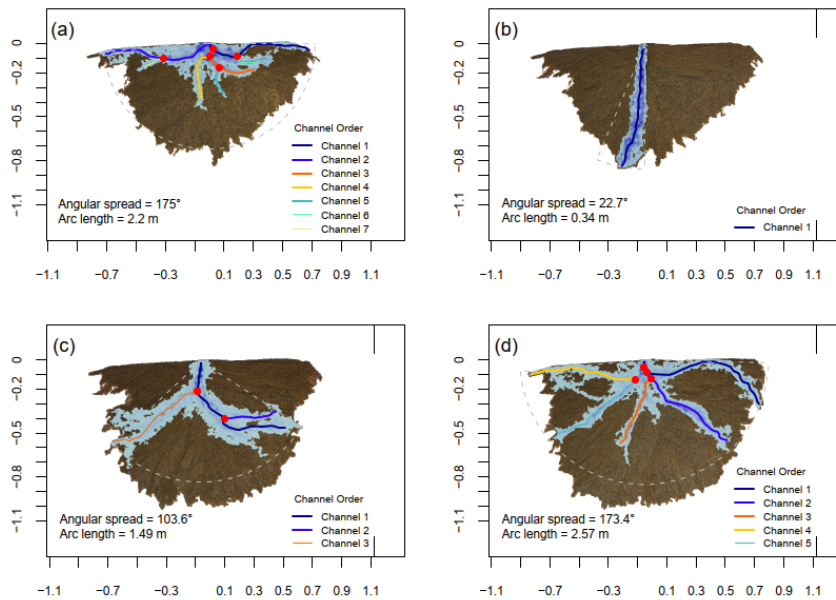
Although discharge and sediment supply were held constant throughout the experiment, the local balance between sediment supply and transport capacity appeared to vary as the channel network reorganized. Because direct measurement of sediment flux or local transport capacity was not feasible in our small-scale physical model, these states are inferred from channel-network configuration, mobility, and reorganization style. When the network expanded across the fan surface, flow was distributed among multiple active threads, which likely reduced the transport capacity of individual channels and promoted sediment storage and reworking across the mid-fan. We interpret these intervals as relatively transport-limited. Examples of relatively transport-limited configurations are shown in Figure 10 a and d, where multiple active channels span a large portion of the fan surface. By contrast, Figure 10 b illustrates a relatively supply-limited, or efficiently connected, configuration, where flow is concentrated in a single dominant channel. Figure 10 c shows an intermediate state. This interpretation is consistent with storage-and-release dynamics documented in previous experimental fan studies [Kim2006; @reitz_experimental_2012; @hamilton_2013].

These inferred states were associated with different styles of channel adjustment. During relatively supply-limited or efficiently connected intervals, flow remained concentrated within a more defined corridor, although this corridor continued to shift laterally through incremental migration. In these intervals,, repeated corridor reworking through successive minor lateral migrations could ultimately produce a net displacement comparable to a single large avulsion. By contrast, during relatively transport-limited intervals, activity was distributed across multiple threads, promoting mid-fan storage and local reworking. These settings favored abrupt, discrete jumps of the main channel. Although some larger avulsions were observed, they were mostly confined to one or two fan sectors rather than extending from the apex to the toe. This behavior aligns with @cazanacli_sediment_2022 and @clarke_experimental_2010, who also documented smaller-scale reorganizations that left large parts of the fan surface unaffected. In our experiment, the nature of channel change was closely tied to the hydraulic regime in the main channel, which alternated between supply-limited and transport-limited conditions. During prolonged supply-limited phases, at least two-thirds of the channel length had sufficient stream power to transport incoming sediment to the fan toe. Any sediment that did accumulate farther down-fan produced only localized impacts, resulting in minimal net aggradation. Consequently, the

Commented [n3]: Change has been made in response to the reviewer's third major comment.

flow remained within a discrete corridor, yet this corridor itself shifted laterally over time through incremental migration. Although major avulsions occurred only infrequently, repeated corridor reworking through successive minor lateral migrations could ultimately produce a net displacement on par with a single large avulsion. In essence, the channel continuously scoured and redeposited local patches of sediment without building up the broad, persistent deposits that would “perch” it to the point of abrupt abandonment. By contrast, transport-limited conditions—where coarser grains accumulated faster than they could be reworked or bypassed—occasionally generated partial super-elevation or localized slope advantages. These settings favored abrupt, discrete jumps of the main channel. Although some full-scale avulsions were observed, they were mostly confined to one or two fan sectors rather than extending from the apex to the toe. This behavior aligns with findings by (Cazanacli, Paola, and Singh 2022) and (Clarke, Quine, and Nicholas 2010), who similarly documented smaller-scale reorganizations that left large parts of the fan surface unaffected.

According to (Mohrig et al. 2000) and (Jerolmack and Mohrig 2007), the time between avulsions in single-thread rivers can be approximated by the formula $T_{\text{avulsion}} = H/V_a$, where H is the channel depth and V_a is the vertical aggradation rate. While this formula offers a useful first-order guide, our experiments show that not all sediment deposition triggers avulsion. Frequent lateral reworking and local bar formation can repeatedly reset channel geometry before the channel becomes fully perched. Consequently, the H/V_a relationship underestimates the importance of small-scale, autogenic adjustments—particularly in highly mobile, widely graded systems where corridor confinement delays or even prevents large-scale avulsions.



Commented [n4]: This figure was added in response to Reviewer's comment to better illustrate the supply-limited and transport-limited interpretations.

Figure 10: Examples of channel-network configurations illustrating the range of the complexity index. (a) $t = 211$ min: seven active channels spanning nearly the full fan width, interpreted as a relatively transport-limited. (b) $t = 225$ min: a single dominant channel occupying a narrow corridor, interpreted as a relatively supply-limited. (c) $t = 317$ min: three channels covering an intermediate portion of the fan surface, representing an intermediate network configuration. (d) $t = 389$ min: five channels distributed broadly across the fan, interpreted as a relatively transport-limited configuration. morphic changes for (a) lateral migration from min 270 to 300 min, and (b) avulsion-dominated phases from 450 and 480 min, both overlaid on a hillshade DEM acquired at the subsequent 30-minute scan.

3.3 Sediment Connectivity and Partial Coupling

Beyond distinguishing lateral migrations from avulsions, our data illustrate how sediment connectivity exerts an important influence on fan dynamics (Harvey, 2010). In natural fan systems, three end-member connectivity states are often cited: buffered systems, where incoming sediment is mainly stored on the fan, leading to high aggradation and minimal sediment export; partially coupled systems, in which some sediment bypasses the fan while the remainder is deposited mid-fan or proximally; and fully coupled systems, where sediment passes freely through the fan, resulting in minimal net storage. Although these concepts are usually discussed in the context of external forcing (tectonics, climate), our

experiments show that autogenic processes operating under constant water and sediment supply can lead the fan to oscillate between more “buffered” and more “partially coupled” states. During supply-limited intervals, the channel appeared to route sediment more efficiently toward the fan toe, consistent with a more partially coupled state; local deposits formed but did not cause significant net aggradation. Conversely, during transient transport-limited phases, coarser grains began to accumulate, producing short-lived “buffering” in specific fan sectors. Occasionally, this buffering was sufficient to trigger abrupt channel jumps. Our results suggest that these oscillations between connectivity states were associated with changes in channel mobility and reorganization style, including transitions between corridor-scale lateral migration and more abrupt, localized channel jumps.

3.4 Role of Widely Graded Sediment in Channel Stability

Although our grain-size distribution was nominally non-cohesive, it differed substantially from the narrowly graded sand mixtures used in previous experiments (Reitz and Jerolmack 2012; Hamilton, Strom, and Hoyal 2013; Reitz, Jerolmack, and Swenson 2010; Carlson et al. 2018). The presence of coarse particles introduced a degree of bed stability, reducing the occurrence of the sheet flow often observed with single-sized sediment (Whipple et al. 1998). Larger clasts nucleated bars and funnelled the flow into channelized corridors rather than allowing it to spread uniformly across the fan surface. These observations align with findings by (Booker and Eaton 2020), (MacKenzie and Eaton 2017), and (MacKenzie, Eaton, and Church 2018), who show that large grains can reduce bed mobility, effectively locking portions of the channel and altering the frequency or style of channel adjustments. In our experiments, this stabilization effect worked in tandem with lower sediment feed rates to facilitate corridor sweeps that continuously eroded and reworked nascent bars, preventing large-scale backfilling. By contrast, (Leenman and Eaton 2021) demonstrated that higher sediment discharge can promote more frequent avulsions; faster aggradation raises the active channel relative to the fan surface, lowering the threshold for abrupt shifts. Thus, even modest differences in sediment supply can tip the balance between stable corridor migration and repeated channel avulsion in systems with wide grain-size distributions (Bryant et al., 1995; Ashworth et al., 2004).

Conclusion

Our experiments on a widely graded, non-cohesive alluvial fan under constant boundary conditions show that channel reorganization can occur through both continuous lateral migration and abrupt avulsive shifts. Using a quantitative classification framework—based on displacement magnitude (relative to channel width) and flow continuity—we differentiate abrupt avulsive from continuous lateral channel shifts, revealing that large net displacements need not arise from singular, fan-wide avulsions. Instead, repeated corridor sweeps can accumulate to match the net effect of a single major jump, indicating how frequent, moderate-scale migrations can dominate fan evolution in highly dynamic, bedload-dominated systems. These findings do not diminish the importance of sediment aggradation or channel perching as mechanisms for avulsion. Rather, they show that

lateral mobility can interact with vertical adjustment by repeatedly redistributing sediment within the active corridor. In this experiment, partial blockage, localized bar formation, and corridor reworking appear to have repeatedly modified channel geometry before a persistent perched configuration developed, suggesting that vertical preconditioning by aggradation and cumulative lateral displacement through migration are not exclusive, and that their relative importance depends on the sediment-flux and lateral-mobility regime of the system. From the perspective of sediment connectivity, our fan oscillated between partially coupled and locally buffered states strictly through internal processes, aligning with previous observations that fans need not rely on external forcing to achieve major reconfigurations. In terms of hazard implications, both corridor sweeps and partial avulsions can affect comparably large areas of the fan. However, the unpredictability of avulsion locations poses a distinct challenge, whereas lateral migration—though still dynamic—tends to remain adjacent to the existing channel, offering somewhat clearer pathways for hazard assessment and mitigation.

Ultimately, our results refine the understanding of alluvial-fan evolution by showing that high lateral mobility and wide grain-size distributions promote incremental corridor reworking, punctuated by occasional abrupt channel jumps. This does not diminish the importance of avulsions for shaping the long-term development and stratigraphic record of major fluvial systems. Instead, it emphasizes that repeated, smaller-scale migrations can significantly redistribute sediment and prolong the interval before an avulsion occurs—especially when total aggradation remains below the threshold set by channel depth. In highly dynamic systems with abundant bedload, these processes can sustain corridor migration and temporarily avoid avulsion. Recognizing the contribution of frequent, moderate-scale reworking and larger, discrete channel shifts is crucial for hazard assessments on modern alluvial fans and for interpreting the sedimentary signatures of ancient fan deposits.

Ashmore, P. 2013. “9.17 Morphology and Dynamics of Braided Rivers.” In *Treatise on Geomorphology*, 289–312. Elsevier. <https://doi.org/10.1016/B978-0-12-374739-6.00242-6>.

Ashmore, Peter E. 1991. “How Do Gravel-Bed Rivers Braid?” *Canadian Journal of Earth Sciences* 28 (3): 326–41. <https://doi.org/10.1139/e91-030>.

Booker, William H., and Brett C. Eaton. 2020. “Stabilising Large Grains in Self-Forming Steep Channels.” *Earth Surface Dynamics* 8 (1): 51–67. <https://doi.org/10.5194/esurf-8-51-2020>.

Bradski, Gary. 2000. “The OpenCV Library.” In *Dr. Dobb’s Journal of Software Tools*.

Bryant, Madeline, Peter Falk, and Chris Paola. 1995. “Experimental Study of Avulsion Frequency and Rate of Deposition.” *Geology* 23 (4): 365–68. [https://doi.org/10.1130/0091-7613\(1995\)023<0365:ESOFA>2.3.CO;2](https://doi.org/10.1130/0091-7613(1995)023<0365:ESOFA>2.3.CO;2).

Bufe, Aaron, Jens M. Turowski, Douglas W. Burbank, Chris Paola, Andrew D. Wickert, and Stefanie Tofelde. 2019. “Controls on the Lateral Channel-Migration Rate of Braided

Channel Systems in Coarse Non-Cohesive Sediment.” *Earth Surface Processes and Landforms* 44 (14): 2823–36. <https://doi.org/10.1002/esp.4710>.

Bull, William B. 1979. “Threshold of Critical Power in Streams.” *GSA Bulletin* 90 (5): 453–64. [https://doi.org/10.1130/0016-7606\(1979\)90<453:TOCPIS>2.0.CO;2](https://doi.org/10.1130/0016-7606(1979)90<453:TOCPIS>2.0.CO;2).

Burge, Leif M. 2006. “Stability, Morphology and Surface Grain Size Patterns of Channel Bifurcation in Gravel–Cobble Bedded Anabranching Rivers.” *Earth Surface Processes and Landforms* 31 (10): 1211–26. <https://doi.org/10.1002/esp.1325>.

Carlson, Brandee, Anastasia Piliouras, Tetsuji Muto, and Wonsuck Kim. 2018. “Control of Basin Water Depth On Channel Morphology and Autogenic Timescales in Deltaic Systems.” *Journal of Sedimentary Research* 88 (9): 1026–39. <https://doi.org/10.2110/jsr.2018.52>.

Cazanacli, Dan, Chris Paola, and Arvind Singh. 2022. “Sediment Load and Grain Size Controls on Channel Migration Patterns in Experimental Deltas.” *Journal of Geophysical Research: Earth Surface* 127 (5): e2021JF006402. <https://doi.org/10.1029/2021JF006402>.

Church, Michael, and Matthias Jakob. 2020. “What Is a Debris Flood?” *Water Resources Research* 56 (8): e2020WR027144. <https://doi.org/10.1029/2020WR027144>.

Clarke, Lucy, Timothy A. Quine, and Andrew Nicholas. 2010. “An Experimental Investigation of Autogenic Behaviour During Alluvial Fan Evolution.” *Geomorphology* 115 (3–4): 278–85. <https://doi.org/10.1016/j.geomorph.2009.06.033>.

Constantine, José Antonio, Thomas Dunne, Joshua Ahmed, Carl Legleiter, and Eli D. Lazarus. 2014. “Sediment Supply as a Driver of River Meandering and Floodplain Evolution in the Amazon Basin.” *Nature Geoscience* 7 (12): 899–903. <https://doi.org/10.1038/ngeo2282>.

Davidson, S. L., and B. C. Eaton. 2018. “Beyond Regime: A Stochastic Model of Floods, Bank Erosion, and Channel Migration.” *Water Resources Research* 54 (9): 6282–98. <https://doi.org/10.1029/2017WR022059>.

Farneback, G. 2000. “Fast and Accurate Motion Estimation Using Orientation Tensors and Parametric Motion Models.” In *Proceedings 15th International Conference on Pattern Recognition. ICPR-2000*, 1:135–139 vol.1. <https://doi.org/10.1109/ICPR.2000.905291>.

Fonstad, Mark A., James T. Dietrich, Brittany C. Courville, Jennifer L. Jensen, and Patrice E. Carbonneau. 2013. “Topographic Structure from Motion: A New Development in Photogrammetric Measurement.” *Earth Surface Processes and Landforms* 38 (4): 421–30. <https://doi.org/10.1002/esp.3366>.

Hamilton, Paul B., Kyle Strom, and David C. J. D. Hoyal. 2013. “Autogenic Incision-Backfilling Cycles and Lobe Formation During the Growth of Alluvial Fans with

Supercritical Distributaries.” *Sedimentology* 60 (6): 1498–1525.
<https://doi.org/10.1111/sed.12046>.

Harvey, Adrian M. 2010. “Local Buffers to the Sediment Cascade: Debris Cones and Alluvial Fans.” In *Sediment Cascades*, 153–80. John Wiley & Sons, Ltd.
<https://doi.org/10.1002/9780470682876.ch6>.

Hooke, Roger. 1968. “Model Geology: Prototype and Laboratory Streams: Discussion.” *GSA Bulletin* 79 (3): 391–94. [https://doi.org/10.1130/0016-7606\(1968\)79\[391:MGPALS\]2.0.CO;2](https://doi.org/10.1130/0016-7606(1968)79[391:MGPALS]2.0.CO;2).

Jerolmack, Douglas J. 2009. “Conceptual Framework for Assessing the Response of Delta Channel Networks to Holocene Sea Level Rise.” *Quaternary Science Reviews* 28 (17–18): 1786–1800. <https://doi.org/10.1016/j.quascirev.2009.02.015>.

Jerolmack, Douglas J., and David Mohrig. 2007. “Conditions for Branching in Depositional Rivers.” *Geology* 35 (5): 463. <https://doi.org/10.1130/G23308A.1>.

Jobe, Zane R., Nick C. Howes, and Neal C. Auchter. 2016. “Comparing Submarine and Fluvial Channel Kinematics: Implications for Stratigraphic Architecture.” *Geology* 44 (11): 931–34. <https://doi.org/10.1130/G38158.1>.

Leenman, Anya, and Brett Eaton. 2021. “Mechanisms for Avulsion on Alluvial Fans: Insights from High-frequency Topographic Data.” *Earth Surface Processes and Landforms* 46 (6): 1111–27. <https://doi.org/10.1002/esp.5059>.

MacKenzie, Lucy G., and Brett C. Eaton. 2017. “Large Grains Matter: Contrasting Bed Stability and Morphodynamics During Two Nearly Identical Experiments.” *Earth Surface Processes and Landforms* 42 (8): 1287–95. <https://doi.org/10.1002/esp.4122>.

MacKenzie, Lucy G., Brett C. Eaton, and Michael Church. 2018. “Breaking from the Average: Why Large Grains Matter in Gravel-Bed Streams.” *Earth Surface Processes and Landforms* 43 (15): 3190–96. <https://doi.org/10.1002/esp.4465>.

Mackey, Scudder D., and John S. Bridge. 1995. “Three-Dimensional Model of Alluvial Stratigraphy; Theory and Applications.” *Journal of Sedimentary Research* 65 (1b): 7–31. <https://doi.org/10.1306/D42681D5-2B26-11D7-8648000102C1865D>.

Martin, John, Ben Sheets, Chris Paola, and David Hoyal. 2009. “Influence of Steady Base-level Rise on Channel Mobility, Shoreline Migration, and Scaling Properties of a Cohesive Experimental Delta.” *Journal of Geophysical Research: Earth Surface* 114 (F3): 2008JF001142. <https://doi.org/10.1029/2008JF001142>.

Miller, Kimberly Litwin, Wonsuck Kim, and Brandon McElroy. 2019. “Laboratory Investigation on Effects of Flood Intermittency on Fan Delta Dynamics.” *Journal of Geophysical Research: Earth Surface* 124 (2): 383–99.
<https://doi.org/10.1029/2017JF004576>.

Mohrig, David, Paul L. Heller, Chris Paola, and William J. Lyons. 2000. "Interpreting Avulsion Process from Ancient Alluvial Sequences: Guadalupe-Matarranya System (Northern Spain) and Wasatch Formation (Western Colorado)." *GSA Bulletin* 112 (12): 1787–1803. [https://doi.org/10.1130/0016-7606\(2000\)112<1787:IAPFAA>2.0.CO;2](https://doi.org/10.1130/0016-7606(2000)112<1787:IAPFAA>2.0.CO;2).

R Core Team. 2025. *R: A Language and Environment for Statistical Computing*. Vienna, Austria: R Foundation for Statistical Computing. <https://www.R-project.org/>.

Reitz, Meredith D., and Douglas J. Jerolmack. 2012. "Experimental Alluvial Fan Evolution: Channel Dynamics, Slope Controls, and Shoreline Growth." *Journal of Geophysical Research: Earth Surface* 117 (F2): 2011JF002261. <https://doi.org/10.1029/2011JF002261>.

Reitz, Meredith D., Douglas J. Jerolmack, and John B. Swenson. 2010. "Flooding and Flow Path Selection on Alluvial Fans and Deltas." *Geophysical Research Letters* 37 (6): 2009GL041985. <https://doi.org/10.1029/2009GL041985>.

Schumm, S. A., M. P. Mosley, and W. Weaver. 1987. "Experimental Fluvial Geomorphology," January. <https://www.osti.gov/biblio/6211294>.

Slingerland, Rudy, and Norman D. Smith. 2004. "RIVER AVULSIONS AND THEIR DEPOSITS." *Annual Review of Earth and Planetary Sciences* 32 (1): 257–85. <https://doi.org/10.1146/annurev.earth.32.101802.120201>.

Sylvester, Zoltán, Paul Durkin, and Jacob A. Covault. 2019. "High Curvatures Drive River Meandering." *Geology* 47 (3): 263–66. <https://doi.org/10.1130/G45608.1>.

Westoby, M. J., J. Brasington, N. F. Glasser, M. J. Hambrey, and J. M. Reynolds. 2012. "'Structure-from-Motion' Photogrammetry: A Low-Cost, Effective Tool for Geoscience Applications." *Geomorphology* 179 (December): 300–314. <https://doi.org/10.1016/j.geomorph.2012.08.021>.

Whipple, Kelin X., Gary Parker, Chris Paola, and David Mohrig. 1998. "Channel Dynamics, Sediment Transport, and the Slope of Alluvial Fans: Experimental Study." *The Journal of Geology* 106 (6): 677–94. <https://doi.org/10.1086/516053>.

Wickert, Andrew D., John M. Martin, Michal Tal, Wonsuck Kim, Ben Sheets, and Chris Paola. 2013. "River Channel Lateral Mobility: Metrics, Time Scales, and Controls." *Journal of Geophysical Research: Earth Surface* 118 (2): 396–412. <https://doi.org/10.1029/2012JF002386>.

Wolman, J.P., M.G.; Miller. 1960. "Magnitude and Frequency of Forces in Geomorphic Processes." *Journal of Geology* 68: 54–74.